Desingularization of ADE Singularities via Deformation

Martina Bátorová *
Comenius University
Bratislava, Slovakia

Miroslava Valíková †
Comenius University
Bratislava, Slovakia

Pavel Chalmovianský ‡
Comenius University
Bratislava, Slovakia

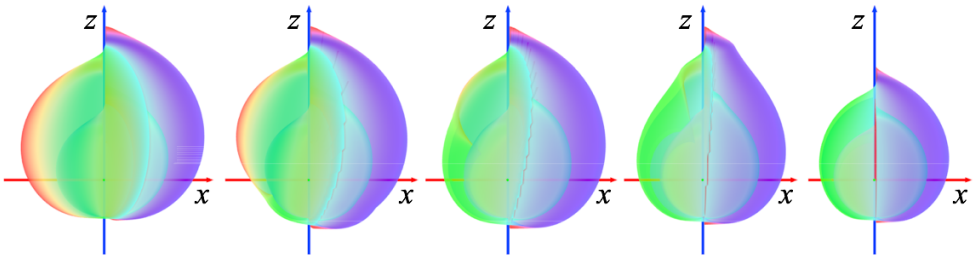

Figure 1: Visualization of passing from the A_2 to A_1 singularity utilizing a 1-parameter deformation.

Abstract

The topology and structure of the ADE singularities in terms of their topological invariants are recalled. A representation of these curves as Riemann surfaces is used to propose a novel technique of visualization of multivalued complex functions. Here, not only the entire domain is displayed, but also the method of domain coloring is extended via utilizing a specific height function. The method is applied in order to show the structure of singularities and to resolve them. A sequence of 1-parameter deformations is used, each causing Milnor number to drop by one up to regularity. The changes in the internal structure are interpreted and the whole process is visualized via computer animation.

CR Categories: G.1.2 [Numerical Analysis]: Approximation—Approximation of Surfaces and Contours; G.1.5 [Numerical Analysis]: Roots of Nonlinear Equations; I.3.7 [Computer Graphics]: Computational Geometry and Object Modeling—Curve, Surface, Solid and Object Representations.

Keywords: visualization, animation, domain coloring, Riemann surface, ADE singularity, torus knot, complex function.

1 Introduction

Today, the area of singularities of algebraic curves is a meeting point of many mathematical disciplines, both theoretical and applied. The interactions and ideas of algebraic geometry, topology, robotics, approximation theory or scientific visualizations – to mention just few – make the subject of the singularities of algebraic curves a very fruitful and exciting field of study.

*e-mail: martina.batorova@fmph.uniba.sk
†e-mail: miroslava.valikova@fmph.uniba.sk
‡e-mail: pavel.chalmoviansky@fmph.uniba.sk

Singular points introduce complications not only in theory, e.g. when computing an image of a curve in a suitable map, but also in practice e.g. in numerical and scientific computations, "division by zero", linear dependence of vectors, discontinuous behavior in certain characteristic values etc. If possible, we wish to eliminate or to avoid them. One way is to replace them locally by a suitable simplification process and to get a curve that no longer contains singularities.

To achieve the goal, we consider the blowup technique and the deformation technique. They consist of multiple steps (e.g. via iteration of a suitable procedure), where the complexity of the assumed singularity is continually reduced. These changes can be captured using special numerical values, called *invariants* that completely characterize the structure and describe the changes of singularity during desingularization.

Such important invariants are the *Milnor number* μ (see sec. 1.1) and torus knot type (see sec. 2.2). We use them to capture the topology and the structure of the *ADE singularities* (see sec. 3). We also utilize a 1-parameter system of deformations (see sec. 5) for their desingularization, each of these deformations causing Milnor number to drop by one up to regularity, i.e. until $\mu = 0$.

We use multiple illustrative techniques of computer graphics. We consider the representation of the curves with ADE singularities as *Riemann surfaces* (see sec. 1.3) to provide a novel technique of visualization of complex functions, creating a tool *CoFiViS* (see sec. 4.2). We also interpret the changes caused by the deformations and demonstrate the whole process using computer animations.

1.1 Basic notions and definitions

We set $\mathbb{N} = \{n \in \mathbb{Z} \mid n > 0\}$ to be the set of positive integers and $\mathbb{N}_0 := \mathbb{N} \cup \{0\}$ the set of the non-negative integers.

Let x, y be indeterminates and let $i, j \in \mathbb{N}_0$. An expression of the form

$$f = f(x,y) = \sum_{i,j \in \mathbb{N}_0} c_{ij} x^i y^j,$$

with $c_{ij} \in \mathbb{C}$, is called a *(formal) power series* over $\mathbb{C}$.

For $f(x,y)$ a non-zero power series, the *support* $\operatorname{supp}(f) := \{(i,j) \in \mathbb{N}_0^2 \mid c_{ij} \neq 0\}$ and the *order* of f is $\operatorname{ord}(f) := \min\{i+j \mid (i,j) \in \operatorname{supp}(f)\}$. We set $\operatorname{supp}(0) = \emptyset$ and $\operatorname{ord}(0) = \infty$.

The usual addition and multiplication of the power series is used and it makes the set of formal power series over $\mathbb{C}$ a commutative ring with 1, denoted $\mathbb{C}[[x,y]]$. Its proper subring of convergent power series is denoted by $\mathbb{C}\{x,y\}$.

We say that the formal power series $f(x,y)$ is a *polynomial* (with coefficients in $\mathbb{C}$) iff $\mathrm{supp}(f)$ is finite. The *degree* of f is defined as

$$\deg(f) := \begin{cases} \max\{i+j \mid (i,j) \in \mathrm{supp}(f)\} & \text{if } f \neq 0, \\ \infty & \text{if } f = 0. \end{cases}$$

A polynomial f is called *homogeneous* of degree d, if all its terms with non-zero coefficients have degree d. Subsequently, every non-homogeneous polynomial $f(x,y)$ of $\deg(f) = d$ can be written as $f(x,y) = f_0(x,y) + \ldots + f_d(x,y)$, where $f_d(x,y)$ is non-zero and each $f_i(x,y)$ is homogeneous of degree i.

Hereditary, the polynomials also form a commutative ring with 1 over $\mathbb{C}$ denoted by $\mathbb{C}[x,y]$, which is a proper subring of $\mathbb{C}[[x,y]]$.

A power series f is said to be *irreducible,* if it cannot be written as a product of two non-constant coprime factors; otherwise it is called *reducible.* The ring $\mathbb{C}[[x,y]]$ is a unique factorization domain, therefore any element f of $\mathbb{C}[[x,y]]$ (and also of $\mathbb{C}[x,y]$) may be uniquely written as $f = c \cdot f_1^{m_1} \cdot \ldots \cdot f_s^{m_s}$, where $c \in \mathbb{C}$ and $f_i(x,y)$ is irreducible, so called *component* or *branch* of f. If $m_i = 1$ for all i, the power series (or polynomial) f is called *square-free* or *reduced*.

1.2 Plane algebraic curves and their local properties

In this paper, we focus on affine plane curves. They are defined as a zero set of an equation $f(x,y) = 0$, where $f\colon \mathbb{A}^2(\mathbb{C}) \to \mathbb{C}$ is a holomorphic function (e.g. polynomial or a power series) in two indeterminates.

The simplest case is when f is a non-constant reduced polynomial, i.e. $f \in \mathbb{C}[x,y]$. The *(affine) plane curve* is $\mathcal{V}(f) := \{(x,y) \in \mathbb{A}^2(\mathbb{C}) \mid f(x,y) = 0\}$. The *degree* of a plane algebraic curve is the degree of its defining polynomial, $\deg(\mathcal{V}(f)) := \deg(f)$. From now on, we only use reduced equations.

We say that the curve $\mathcal{V}(f)$ is *irreducible*, if it cannot be written as a union of two curves of strictly lower non-zero degree; otherwise, it is *reducible*. Every curve can be uniquely written as a finite union $\mathcal{V}(f) = \mathcal{V}(f_1) \cup \ldots \cup \mathcal{V}(f_s)$ of irreducible curves $\mathcal{V}(f_i)$ such that $\mathcal{V}(f_i) \subsetneq \mathcal{V}(f_j)$ for $i \neq j$. The sets $\mathcal{V}(f_i)$ are called the *(irreducible) components* or *branches* of $\mathcal{V}(f)$. Moreover, $f = f_1 \cdot \ldots \cdot f_s$ is the factorization of f.

A complex function of two complex variables, defined on some neighborhood $\mathcal{U} \subset \mathbb{C}^2$ of the origin $O := (0,0)$, is called *holomorphic* or *(complex) analytic on $\mathcal{U}$,* if it can be expanded to a convergent power series (Taylor expansion) in $\mathcal{U}$. In particular, given $f \in \mathbb{C}\{x,y\}$ such that $f(O) = 0$, there is a (Euclidean) neighborhood $\mathcal{U} \subset \mathbb{C}^2$ of $O \in \mathcal{U}$ such that $f(x,y)$ converges. Therefore, the equation $f(x,y) = 0$ defines a restriction of the curve $\mathcal{V}(f)$ in $\mathcal{U}$. This enables us to define a local equivalence of plane algebraic curves.

Let $f_1\colon \mathcal{U}_1 \to \mathbb{C}$ and $f_2\colon \mathcal{U}_2 \to \mathbb{C}$ be two functions defined on the (Euclidean) neighborhoods $\mathcal{U}_1, \mathcal{U}_2$ of the point $O \in \mathbb{C}^2$ such that $f_1(O) = f_2(O) = 0$. We say that functions f_1, f_2 define the same *germ at the point O,* if they coincide on some neighborhood $\mathcal{U} \subset \mathcal{U}_1 \cap \mathcal{U}_2$ of O. In case of holomorphic functions, this holds iff the power series expansions of f_1, f_2 at O coincide.

The affine plane curve $\mathcal{V}(f) \subset \mathbb{A}^2(\mathbb{C})$ consists of two types of points. The point $P \in \mathcal{V}(f)$ is called a *singular point (singularity)* of $\mathcal{V}(f)$, if both partial derivatives $\frac{\partial f}{\partial x}, \frac{\partial f}{\partial y}$ vanish at P. A point which is not singular is called *regular*. We say that the curve $\mathcal{V}(f)$ is *regular* or *smooth* if all its points are regular, otherwise it is called *singular*. From now on, we assume the singularity to be placed at the origin O. Clearly, this can always be achieved by a linear coordinate change.

Let $f(x,y) = f_m(x,y) + \ldots + f_d(x,y)$ and $f_i(x,y)$ be its homogeneous part of degree i, with f_m, f_d non-zero. If $O \in \mathcal{V}(f)$, $m \geq 1$ and if it is singular, $m \geq 2$. In either case, the polynomial f_m factorizes into m linear components, each defining a *tangent* to $\mathcal{V}(f)$ at O. The set of all such tangents is called the *tangent cone* of $\mathcal{V}(f)$ at O.

A singularity $P \in \mathcal{V}(f)$ of the reduced plane algebraic curve $\mathcal{V}(f)$ can be only *isolated* ones, hence there exists a neighborhood $\mathcal{U}$ such that $\mathrm{Sing}(\mathcal{V}(f)) \cap (\mathcal{U} \setminus \{P\}) = \emptyset$, where $\mathrm{Sing}(\mathcal{V}(f))$ denotes the set of all singular points of $\mathcal{V}(f)$.

Isolated singular points can be classified according to their internal structure upto isomorphism. This structure varies from very simple, e.g. so called *ordinary* (having only different non-multiple tangents to the curve at the corresponding point) to more complicated ones. The complexity of singularities can be measured via so called *invariants*, which are intristic values (numbers, rings etc.) of the curve.

The *Milnor number* μ is one of the most important of such invariants. It may be defined in various ways, depending whether we wish to emphasize its topological, algebraic or geometrical interpretation; we choose the latter.

Let $\mathcal{V}(f) \subset \mathbb{C}^2$. The ideal $J(f) := \left\langle \frac{\partial f}{\partial x}, \frac{\partial f}{\partial y} \right\rangle$ in the ring $\mathbb{C}\{x,y\}$ is called the *Jacobi ideal* of f. The *Milnor number $\mu(f)$ of $\mathcal{V}(f)$* at the origin is the dimension of $\mathbb{C}\{x,y\}/J(f)$ considered as a $\mathbb{C}$-vector space. If $\mathcal{V}(f)$ is a smooth branch, $\mu(\mathcal{V}(f)) = 0$. If it is singular at O, the Milnor number is finite, because O is an isolated singularity of $\mathcal{V}(f)$. In particular, if $\mathcal{V}(f)$ is irreducible, $\mu(\mathcal{V}(f))$ is even, otherwise odd. Moreover, we can break up any isolated singularity into μ distinct ones, each with $\mu = 1$ (see e.g. A_1 in fig. 2). These new singularities are very simple, each is the union of two smooth branches meeting transversely ([Wall 2004]).

For more information on the subject of plane algebraic curves see [Greuel et al. 2007], [Wall 2004], [Brieskorn and Knörrer 1986].

1.3 Riemann surfaces

The concept of Riemann surfaces is fundamental in modern complex analysis, topology and algebraic geometry. Moreover, such surfaces are utilized also in several methods in computer graphics. For example, [Yin et al. 2007] uses the universal covering to compute the shortest cycles in each homotopy class of given surface.

In this paper, we use Riemann surfaces for representation of complex plane curves, as the complex curve $\mathcal{V}(f) \subset \mathbb{C}^2$ can be considered as a real surface in $\mathbb{R}^4 \cong \mathbb{C}^2$, picturing them in one's mind is not so natural as in case of real curves. Here, we give a short mathematical background on Riemann surfaces, techniques developed for their visualization are described in sec. 4.2.

Let X be a two-dimensional manifold. A *complex chart* on X is a pair (U, ϕ), where $\phi\colon U \to V$ is a homeomorphism and $U \subset X$ and $V \subset \mathbb{C}$ are open subsets. Two complex charts $\phi_i\colon U_i \to V_i$, $i = 1,2$ are said to be *holomorphically compatible* if the map

$$\phi_2 \circ \phi_1^{-1}\colon \phi_1(U_1 \cap U_2) \to \phi_2(U_1 \cap U_2)$$

is biholomorphic.

A *complex atlas on* X is a system of complex charts $\mathscr{U} = \{(U_i, \phi_i) \colon U_i \subset X, \phi_i \colon U_i \to V_i, i \in I\}$, which are holomorphically compatible and form a cover of X, i.e. $\bigcup_{i\in I} U_i = X$. Two complex atlases $\mathscr{U}$ and $\mathscr{U}'$ on X are *analytically equivalent,* if every chart of $\mathscr{U}$ is holomorphically compatible with every chart of $\mathscr{U}'$. By a *complex structure* on a 2-dimensional manifold X we mean an equivalence class of analytically equivalent atlases on X. Thus a complex structure on X can be given by a choice of the complex atlas.

A *Riemann surface* is a pair $(X, \mathscr{S})$, X being a connected 2-dimensional manifold and $\mathscr{S}$ a complex structure on X.

Suppose X and Y are topological spaces. A mapping $p \colon Y \to X$ is called a covering map, if every point $x \in X$ has an open neighborhood U such that its preimage $p^{-1}(U)$ can be represented as $p^{-1}(U) = \bigcup_{j\in J} V_j$, where the V_j, $j \in J$, are disjoint open subsets of Y, and all the mappings $p|_{V_j} \colon V_j \to U$ are homeomorphisms [Lang 1999]. Suppose X, Y are Hausdorff spaces with X pathwise connected and $p \colon Y \to X$ is a covering map. Then for any two points $x_0, x_1 \in X$ the sets $p^{-1}(x_0)$ and $p^{-1}(x_1)$ have the same cardinality. In particular, if Y is non-empty, then p is surjective. The cardinality of $p^{-1}(x)$ for $x \in X$ is called the *number of sheets* of the covering and may be either finite or infinite.

A *meromorphic* function $f \colon \Sigma \to \Sigma$ is a function that is holomorphic on whole Σ except a set of isolated points, which are poles of the function, i.e. f is meromorphic iff it is a rational function.

Assume that X and Y are Riemann surfaces and $p \colon X \to Y$ is a non-constant holomorphic map. A point $y \in Y$ is called a *branch point* or *ramification* of p, if there is no neighborhood V of y such that $p|_V$ is injective. A *branch cut* L is a curve joining two branch points in the complex plane. If we cut Σ along simple mutually disjoint paths between pairs of branch points of the function f, we get a simply connected region on which we can define a singlevalued meromorphic branch of the multivalued function.

2 Topology of plane curve singularities

2.1 Puiseux expansion. Characteristic exponents.

Let $f(x,y) = \sum_{i,j\in\mathbb{N}_0} c_{ij} x^i y^j, c_{00} = 0$ be a power series. The formal power series $f(x,y)$ is called a *y-general of order m,* if $f(0,y) = cy^m +$(terms in y of higher degree), $c \in \mathbb{C} \setminus \{0\}$, i.e. if $c_{0m} \neq 0$ and $c_{0j} = 0$ for all $j < m$.
The y-generality of finite order simply means that the y-axis is not a tangent to $\mathcal{V}(f)$ at origin. Clearly, this situation can always be achieved by a linear coordinate change ([Greuel et al. 2007]).

If $f \in \mathbb{C}[[x,y]]$ is irreducible and y-general of order m, then there exists $g(t) \in \mathbb{C}\{t\}, g(t) = \sum_{i\geq m} a_i t^i$ such that $f(t^m, g(t)) = 0$. Moreover, $t \to (t^m, g(t))$ is a parameterization of f ([Greuel et al. 2007]). Thus, for a point $(x,y) \in \mathcal{V}(f)$, we have $x = x(t) = t^m, y = g(t) = g(x^{\frac{1}{m}}) = \sum_{i\geq m} a_i x^{\frac{i}{m}}$. The fractional power series $g(x^{\frac{1}{m}}) \in \mathbb{C}\{x^{\frac{1}{m}}\}$ is called the *Puiseux expansion of* f. Such an expression can be acquired via the *Newton-Puiseux algorithm* [Greuel et al. 2007; Wall 2004; Brieskorn and Knörrer 1986], where the power series $g(t)$ of the parameterization is constructed inductively in a sequence of steps, term by term.

It is important to note, that we construct only *local parameterizations*, i.e. parameterizations of a curve branch upto the next singularity. Also, we may construct the parameterization of f using $n > m$, but using minimal such m, i.e. utilizing the y-generality, defines so called *good parameterization* of $\mathcal{V}(f)$, where to each point of f corresponds only one value of t – which has many useful and convenient consequences. Therefore from now on, we shall use only good parameterizations.

Let $g(x^{\frac{1}{m}}) = \sum_{i\geq m} a_i x^{\frac{i}{m}}$ be a Puiseux expansion corresponding to a good parameterization $(t^m, g(t))$ of $f(x,y)$ and assume that not all exponents are integers. Then there is a smallest $k_1 = \frac{n_1}{m_1} \in \mathbb{Q} \setminus \mathbb{Z}$ s.t. n_1, m_1 are coprime and $n_1 > m_1 > 1$. The pair (m_1, n_1) is called the *first Puiseux pair* of f. If not all of the following exponents are of the form $\frac{q}{m_1}, q > n_1$, the number $k_2 = \frac{n_2}{m_1 m_2}$ with n_2, m_2 coprime and $m_2 > 1$ exists and (m_2, n_2) is called the *second Puiseux pair*. In general, if the Puiseux pairs $(m_1, n_1), \ldots, (m_i, n_i)$ are already defined, then k_{i+1} is the smallest exponent for which the preceding exponents are expressible in the form $\frac{p}{m_1 \cdot \ldots \cdot m_i}$ and k_{i+1} cannot be so. Then $k_{i+1} = \frac{n_{i+1}}{m_1 \cdot \ldots \cdot m_{i+1}}$, where n_{i+1} and m_{i+1} are coprime and $m_{i+1} > 1$ and (m_{i+1}, n_{i+1}) is the $(i+1)$*st Puiseux pair.* This process always terminates and we get a finite sequence $(m_1, n_1), \ldots, (m_r, n_r)$ of integer *Puiseux pairs*.

Using a similar reasoning, we construct a special sequence of positive integers $(m; \beta_1, \ldots, \beta_r)$ via setting

$$\begin{aligned} \beta_1 &= \min\{k \mid a_k \neq 0, m \nmid k\} \qquad e_1 = \gcd(m, \beta_1), \\ \beta_i &= \min\{k \mid a_k \neq 0, e_{i-1} \nmid k\} \quad e_i = \gcd(e_{i-1}, \beta_i) \end{aligned}$$

with $i = 2, \ldots, r$ s.t. $e_r = 1$. The algorithm always terminates, as the parameterization $g(t)$ was assumed to be good.

The sequence $(m; \beta_1, \ldots, \beta_r)$ is called the *Puiseux characteristic* of f, the numbers β_i are the *characteristic exponents* and the sequence $(e_0; e_1, \ldots, e_r)$ with $e_0 := m$ is the *associated Puiseux sequence*. It can be proven that the characteristic is independent of the choice of coordinates [Wall 2004].

The Puiseux pairs and the Puiseux characteristic with its associated Puiseux sequence are for $i = 1, \ldots, r$ interrelated via the following formulae [Greuel et al. 2007]:

$$\begin{aligned} m &= m_1 \cdot \ldots \cdot m_r & m_i &= \frac{e_{i-1}}{e_i} \\ \beta_i &= \frac{m n_i}{m_1 \cdot \ldots \cdot m_i} & n_i &= \frac{\beta_i}{e_i}. \end{aligned} \tag{1}$$

2.2 Cable knots

A complex curve $\mathcal{C} \subset \mathbb{C}^2$ can be considered as a real surface in $\mathbb{R}^4 \cong \mathbb{C}^2$. Its intersection $\mathcal{K}$ with a small sphere $\mathbb{S}^3_\varepsilon$ around the singularity is called a *knot* associated to a singularity of $\mathcal{C}$: $\mathcal{K} = \mathcal{C} \cap \mathbb{S}^3_\varepsilon$. The knot is independent of the sphere radius ε for sufficiently small $\varepsilon > 0$ [Brieskorn and Knörrer 1986]. For a plane curve singularity, there is a nice description of the knot structure called the *cable knot* or the *iterated torus knot* [Wall 2004],[Greuel et al. 2007].

If $(x,y) = (t^m, g(t))$ is a good parameterization of the branch $\mathcal{V}(f)$, then for each x we have at most m values of y. Therefore, f can be written as

$$(x,y) = u(x,y) \prod_{i=1}^{m} \left(y - y\left(\xi^i x^{\frac{1}{m}}\right)\right),$$

where ξ is a primitive m-th root of 1 and $u \in \mathbb{C}\{x,y\}$ is a unit.

The knot equation of a plane curve singularity has the form

$$x(t) = t^m, \quad y(t) = a_1 t^{\beta_1} + \ldots + a_r t^{\beta_r},$$

where $(m; \beta_1, \ldots, \beta_r)$ is the Puiseux characteristic and $a_1, \ldots, a_r \in \mathbb{C}$ are non-zero and properly picked, see e.g. fig. 4 (left). This is isotopic to a real knot on the surface.

Now, if t is viewed as a path around a circle $\mathbb{S}^1_\rho$ with radius $\rho := \sqrt[m]{\delta} > 0$, then $t = \rho e^{i\theta}, \theta \in \langle 0, 2\pi \rangle$. The image of the knot is given by

$$x(\theta) = \delta e^{im\theta}, \quad y(\theta) = a_1 \sqrt[m]{\delta^{\beta_1}} e^{i\beta_1\theta} + \ldots + a_r \sqrt[m]{\delta^{\beta_r}} e^{i\beta_r\theta}. \quad (2)$$

We see that the graph of the m-valued function $y(t)$ are projections of m copies of $\mathbb{S}^1_\rho$ onto the cylinder $\mathcal{Q} \equiv \mathbb{S}^1_\rho \times \mathbb{C} = \{(x,y) \colon |x| = \sqrt[m]{\delta}\}$.

Both the coordinates x, y in equation (2) are cyclic, therefore we can conveniently graph them on a torus. This also enables us to give the following geometric interpretation of the previous knot construction. We start with a simple (untied) knot $\mathcal{K}_0 \cong \mathbb{S}^1_\varepsilon$ and consider the surface of its small tubular neighborhood, i.e. a torus $\mathcal{T}_0$. Now we construct a new knot $\mathcal{K}_1$ lying on $\mathcal{T}_0$ so that the coordinate x represents wrapping m times around the parallels and the coordinate y wrapping β_1 times around the meridians of $\mathcal{T}_0$. If the singularity is more complicated, i.e. the Puiseux characteristic has $r > 1$ terms, we construct another tubular neighborhood $\mathcal{T}_1$ of $\mathcal{K}_1$ and a new knot $\mathcal{K}_2$ lying on $\mathcal{T}_1$. This knot is again determined by two integers specifying how many times it must turn around $\mathcal{T}_1$ in either direction. It turns out that these two numbers are given exactly by the next Puiseux pair $(m_2, n_2) = \left(\frac{e_1}{e_2}, \frac{\beta_2}{e_2}\right) = \left(\frac{\gcd(m,\beta_1)}{\gcd(m,\beta_1,\beta_2)}, \frac{\beta_2}{\gcd(m,\beta_1,\beta_2)}\right)$, see equation(1). The final knot is constructed via a r-step iteration of the previous procedure, when if $\mathcal{T}_i$ is a torus for the first i terms in equation (2), adding of the $(i+1)$st term produces a knot of type $\left(\frac{e_i}{e_{i+1}}, \frac{\beta_{i+1}}{e_{i+1}}\right)$. The construction also explains the name cable knot and iterated torus knot.

3 ADE singularities

In this paper, we focus on a very special kind of hypersurface singularities, the so called *ADE* or *simple* singularities [Greuel et al. 2007]. They are isolated and additionally, their internal (topological) structure is very simple, e.g. they are describable by a single Puiseux pair, which indicates the least complicated type of isolated singularities. The *ADE* string itself is a standard Vladimir Arnold's notation for simple singularities. It is based on the deep connection of these singularities with simple Lie groups, where each of the A-D-E denotes the corresponding Lie algebra.

In the plane case, the ADE singularities are defined as zero sets of $f \in \mathbb{C}[x,y]$ or $f \in \mathbb{C}[[x,y]]$, where f has on of the following forms:

$$\begin{array}{llll} A_k\colon & x^{k+1}+y^2 & k \geq 1 & \qquad E_6\colon \quad x^4+y^3 \\ D_k\colon & x(x^{k-2}+y^2) & k \geq 4 & \qquad E_7\colon \quad y(x^3+y^2) \\ & & & \qquad E_8\colon \quad x^5+y^3, \end{array} \quad (3)$$

see fig. 2, 3 for depiction of the real parts of several of the ADE curves in a properly chosen coordinate system. The classification is valid upto a coordinate change, for more see [Wall 2004], [Greuel et al. 2007].

For k odd, the plane curves with the A_k singularity are reducible – they comprise of two lines or two generalized parabolas. The plane D_k singularities are all reducible – they consist of the y axis and the A_{k-3} singularity. The E_6 and E_8 singularities are irreducible, the E_7 one is not.

The parabola $A_0\colon x+y^2$ is usually excluded, since it is regular. The $A_1\colon x^2+y^2$ singularities are called *nodes*, the $A_2\colon x^3+y^2$ singularities *cusps*.

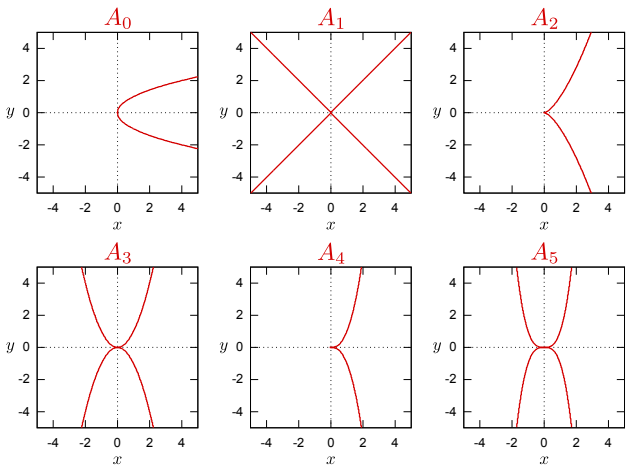

Figure 2: Real locus of some of the complex plane A_k singularities, including the regular parabola A_0.

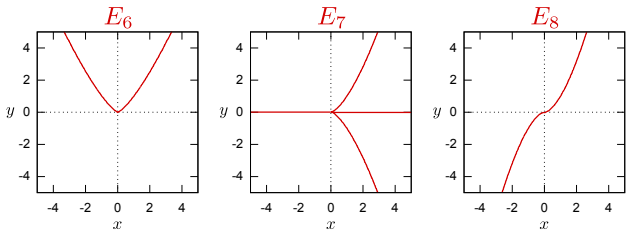

Figure 3: Real locus of some of the complex plane E_6, E_7, E_8 singularities.

The ADE singularities are of a very special kind, either of so called *toric* or *quasitoric* type [Hasset 2000].

Let $p \geq q > 1$ be integers. A plane curve singularity $\mathcal{V}(f)$ is said to be of *toric type* (q,p), if it has the same topological type as $x^p + y^q$, i.e. it is representable in such a way in a suitably chosen coordinate system. The singularity $\mathcal{C}$ is of a *quasitoric type,* if it has the topological type as one of the following:

$$\begin{array}{rl} x(x^p+y^q) & \text{with } p > q, \\ y(x^p+y^q) & \text{with } p > q \text{ and } q \nmid p, \\ xy(x^p+y^q) & \text{with } p > q \text{ and } q \nmid p. \end{array}$$

We see that the A_k and D_4 singularities are of the toric type, the $D_k, k > 4$ of the quasitoric type, the E_k singularities of the toric (E_6, E_8) and the quasitoric type (E_7).

The numbers (q,p) represent precisely the torus knot type of given singularity and thus also their topology. In fig. 4, we see knots for each of the A_2, A_4, A_6, E_6, E_8 plane singularities. Their respective Puiseux pairs are $A_2\colon (2,3)$ (the *trefoil* knot), $A_4\colon (2,5)$ (the *cinquefoil* knot), $A_6\colon (2,7)$, $E_6\colon (3,4)$ and $E_8\colon (3,5)$. The A_k for k odd are not given, because the curve factorizes into regular factors and thus the knots of respective branches are trivial, the D_k singularities are a union of the y-axis and the A_{k-3} singularity (their knot is a union of the trivial and the $(2,k-2)$-knot), and the E_7 is of the same topological type as the union of the x-axis and the A_2 singularity (its knot is the union of the trivial and the trefoil knot).

In all the cases, the indices $k, 6, 7, 8$ refer to the Milnor number μ of given ADE singularity. This invariant is for the toric and quasitoric,

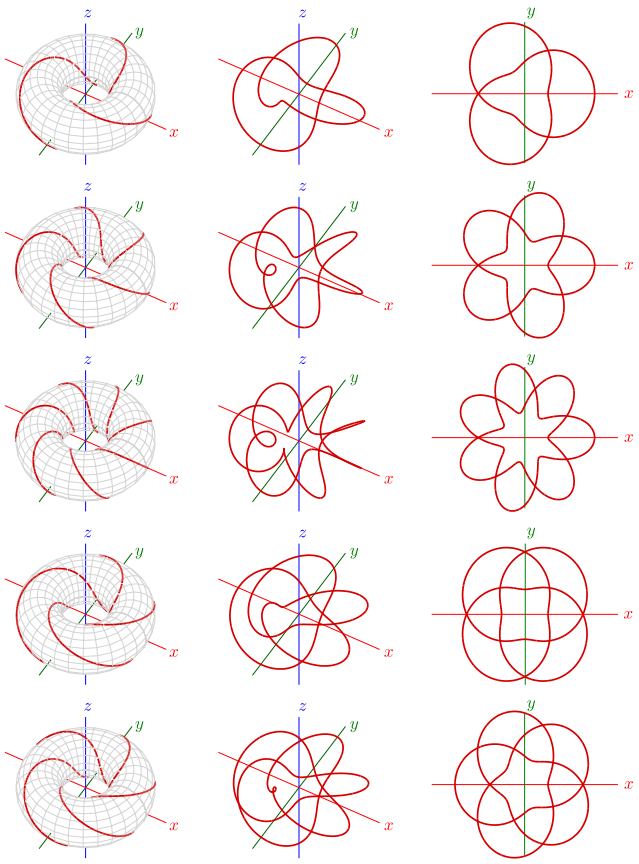

Figure 4: Figures of the knots associated to the A_2, A_4, A_6, E_6, E_8 singularities, from left to right: the torus knot depicted on the $\mathcal{T}_0$ torus (left), the knot itself (middle) and the projection to the (x,y)-plane (right).

and thus for the ADE singularities as well, computed as follows:

$$\mu(x^p + y^q) = (p-1)(q-1),$$
$$\mu(x(x^p + y^q)) = (p-1)(q-1) + 2q - 1$$
$$\mu(y(x^p + y^q)) = (p-1)(q-1) + 2p - 1.$$

4 Visualization of complex functions

To visualize a real function $f\colon \mathbb{R} \to \mathbb{R}$, we draw a graph $y = f(x)$ in a two dimensional Cartesian coordinate system in $\mathbb{R}^2$ via identifying one axis with the domain of the function and the other axis with its codomain. This method meets with some difficulties when we want to extend it to a complex function $g\colon \mathbb{C} \to \mathbb{C}$. The main problem arising is that $\mathbb{C}$ has a real dimension 2, thus we need a 4-dimensional real space to depict the graph of a complex function $w = g(z)$.

The plane complex curves can be naturally represented as Riemann surfaces. However, there are only few publications on their computer-aided visualization. Some work has been done by Trott for *Wolfram Research*. In the paper [Trott 2002], the symbolic derivation and nonlinear equations solver provided by *Mathematica* [Wolfram Research 2013] was used to compute 3D plots based on an explicit function definition. The most recent work [Nieser et al. 2010] deals with automatic generation of Riemann surfaces.

4.1 Domain coloring

One of the newest approaches to visualization of complex functions is the *domain coloring*. This method was introduced by Frank A. Farris on his webpage [Farris 2012]. Farris's method comprises of two main steps: 1. color the codomain w, this may also utilize a random image or a parametric texture, 2. assign a corresponding color of $f(z)$ to each point z of the domain.

Another variation of domain coloring can be found in [Lundmark 2004]. The author picks a continuous radial color gradient with center at the origin of the polar coordinate system that assigns a unique color to every value of the angle.

One of the latest methods of visualizations of complex functions with domain coloring was published in [Poelke and Polthier 2009] and it works as follows. We work on the unit ball $\mathbb{B}_1$ given by a parameterization $\mathbb{B}_1 = \{(r\cos\phi\cos\theta, r\cos\phi\sin\theta, r\sin\phi) \mid 0 \le r \le 1; \phi \in \langle 0, \pi\rangle, \theta \in \langle 0\ 2\pi\rangle\}$. To define the color gradient, we assign the HSB color gradient as follows: the color tone corresponds to the angle θ, the tint to the radius r and the brightness defines the angle ϕ. We compose the coloring function col into two functions $col = c \circ p$, where $c\colon \mathbb{B}_1 \to HSB$, $p\colon V \to \mathbb{B}_1$ and V being the codomain of the visualized function. The function c is defined in such a way that the south pole of the sphere $\mathbb{B}_1$ is black, the equator has color with the maximum tint and brightness and the north pole is white. As the function p may be chosen e.g. the inverse of the stereographic projection, which in the black color is assigned to the point 0 and the white color to ∞. Also, we wish the gradient to be continuous and to engage the whole color spectrum. This work flow can be used to color Riemann surfaces (see sec. 1.3) or any other parameterized regular surface.

Via the coloring, we are able to detect visually zeros and poles of given function. We can also see the deformation of the domain of the function. So far, we cannot determine the velocity of the value of the absolute value of the function f. We can only ascertain the direction of the growth from 0 to ∞. Therefore semitransparent layer with concentric circles and a repeating grayscale gradient is used in [Lundmark 2004]. To determine the radius of the circles, the logarithmic function was used. This gives an exponential growth of the radius. In the end, k half-lines are drawn, starting in 0 and intersecting the k-th root of unity. Moreover, it is possible e.g. to find out whether the given function preserves angles or not via the obtained grid [Poelke and Polthier 2009].

4.2 CoFiViS: Visualization of Riemann surfaces

We created the *CoFiViS* tool for visualization of Riemann surfaces using the open source program *Blender* [Blender 2013]. It can be used to create 3D models, animations and games. Incorporated scripting language *Python* [Python 2012] enables the user to utilize predefined functionality and define new one. At the present time, the implementation of CoFiViS is still in progress, it is a part of the Dissertation Thesis of the second author. It will be available online after the Thesis defense, not later than April 2014.

At first, we present a simple example of a multivalued function, the square root $f(z) = \sqrt{z}$. This function has two branches, because the square root assigns to one point $p \neq 0$ two different values, see fig. 5. These two values can be calculated using the goniometric form of the complex number: if $z = re^{i\phi}$, the square root of z is $\sqrt{z} = \sqrt{r}e^{i(\phi/2)}$, where $\sqrt{r}$ is the real square root of the distance of the point z from 0.

To start with, we choose $\sqrt{p} = a$, see fig. 5, top. If we move along a path A, starting and ending at the point p and not containing 0,

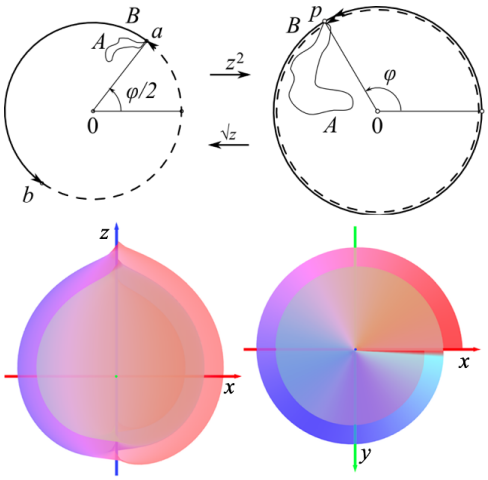

Figure 5: The top figures give evidence that the square root of a complex number $p \neq 0$ has two different values a, b. The bottom figures display the Riemann surface of the square root from two different points of view.

the image of the path will start and end at the point a. If we move along the circle B from the point p around 0 again to p, the image of the circle will start at the point a and end at the point b. We get to the point a after second round around 0 along the circle B. This is due to the fact that the point 0 is a branch point of the function $f(z) = \sqrt{z}$.

The Riemann surface of the square root is constructed as follows. First we choose the branch cut. Here, we choose the ray $l = \{z \in \mathbb{R}; z \geq 0\}$. The complement is set $E = \mathbb{C} \setminus l$. As the square root assigns two images to one preimage, we need 2 copies of the set E, denoted E_0, E_1, with their branch cuts l_0, l_1. Next, we connect these copies along the branch cuts. The Riemann surface of the square root is displayed in fig. 5, bottom.

In this paper, we visualize Riemann surfaces $\mathscr{S}$ of $\sqrt{p(z)}$, where $p(z) = \prod_{j=1}^{m}(z-a_j)^{b_j}$ is a polynomial and $a_1, \ldots, a_m$ are all distinct (see 3). If the multiplicities b_j of the roots a_j of p are all even, there are two single-valued meromorphic branches $f_1(z) = \prod_{j=1}^{m}(z-a_j)^{b_j/2}$ and $f_2(z) = -f_1(z)$ of $\sqrt{p}$, so the Riemann surface $\mathscr{S}$ of $\sqrt{p}$ is a disjoint union of two spheres, each being a domain of the branch f_i. The Riemann surface $\mathscr{S}$ of $\sqrt{p}$ consists of two copies of the region $E = \Sigma \setminus L$, denoted E_1 and E_2, the domains of f_1, f_2 respectively. Since we cannot pass from one branch to another by a meromorphic continuation of $\sqrt{p}$, we do not join E_1 and E_2, but instead we regard the surface $\mathscr{S}$ as a 2-sheeted unbranched covering surface of Σ consisting of two disjoint spheres.

Hence, we assume that the multiplicity b_j of some root a_j of p is odd. We write $\sqrt{p} = q\sqrt{r}$, where q and r are polynomials, and r is non-constant and squarefree. Since q is a singlevalued and meromorphic on Σ, the construction of the Riemann surface of $\sqrt{p}$ is topologically identical to that of $\sqrt{r}$. That means, the crossing of the layers and the position of branch points are the same. Therefore by replacing p by r we may assume that p has distinct roots and is not constant, i.e. $m \geq 1$ and each $b_j = 1$.

If m is even ($m = 2k$), $a_1, \ldots, a_m$ are the only branch points, but if m is odd ($m = 2k-1$), there is a branch point lying over $a_{2k} = \infty$. In either case, there is an even number of branch points over $a_1, \ldots, a_{2k}$, so we cut $\Sigma = \mathbb{C} \cup \{\infty\}$ along simple mutually disjoint paths from a_1 to a_2, a_3 to $a_4, \ldots, a_{2k-1}$ to a_{2k} and get a region E. The Riemann surface $\mathscr{S}$ can be formed by taking E_1, E_2, each being a domain of a meromorphic branch of $\sqrt{p}$, and joining E_1 to E_2 along lines lying above the k cuts in Σ. This gives us a 2-sheeted surface $\mathscr{S}$ of Σ, homeomorphic to a sphere with $k-1$ handles attached [Jones and Singerman 1987].

The function $\sqrt{p(z)}$ has two branches, as the polynomial $p(z)$ is a single-valued function and the second root is a 2-valued function. In the first step, we created two approximations of the unit sphere with center at the origin $(0,0,0)$ parameterized as $\mathbb{S}^2 = \{(\cos(t)\cos(u), \cos(t)\sin(u), \sin(t)) \mid t \in \langle \frac{\pi}{2}, \frac{\pi}{2} \rangle, u \in \langle 0, 2\pi \rangle\}$.

In CoFiViS, the user can also choose the level of detail of the approximation, in particular, the global number of vertices.

Utilizing the color gradient method, we change the position and color of the vertices according to the value of the function [Valíková and Chalmovianský 2010]. At first, we compute the coordinate of the vertex in the complex plane via the inverse stereographic projection [Jones and Singerman 1987]. The complex number $z = a + bi$ assigned to each vertex is represented in its goniometric form $z = re^{i\phi}$ and substituted into the function formula. The color gradient, see fig. 6, presents the values of the argument of the function.

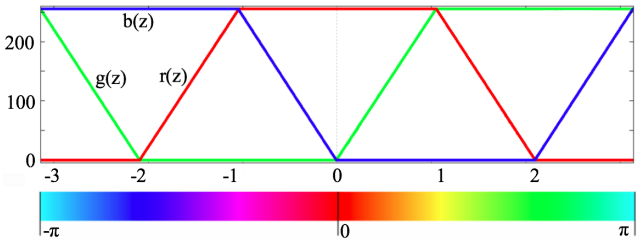

Figure 6: Visualization of the value of the argument of the function $f(z)$ via color gradient.

After assigning color to all the vertices of the first layer, the program proceeds to the second layer. The second branch of the function is given by formula $-f(z)$. At first, the two layers coincide. To separate them, we change the distance of the vertices from the point $(0,0,0)$. The distance is calculated using the modulus of the function multiplied by the argument of the value of the function. This causes the singular points, or so called roots of the polynomial to lie on the domain sphere with the radius $r = 1$. In the end, the first layer lies in a different distance from the origin as the second layer.

During the implementation, certain inaccuracies appeared. Few layers were connected improperly, see fig. 7. This was caused by the change of the number of roots which are encircled by the vertices, which are on the same plane parallel to plane given by axes x and y. Therefore, we used the linear interpolation method to connect them properly. There was a sudden change in the color is caused by the implementation of the argument of the complex number by *Python*. We corrected it by swapping the corresponding part of the first layer with second layer.

4.3 Interpretation of visualizations

To provide the reader with a detailed interpretation of the figures, we choose visualization of the function $f(z) = \sqrt{-z^3}$, see fig. 8.

We see the graph of the function $f(z)$ from two different points of view. In the left figure, the direction of the camera corresponds to the y-axis (the front view). In the right one, the direction corresponds to the negative z-axis (view from the top). The left figure

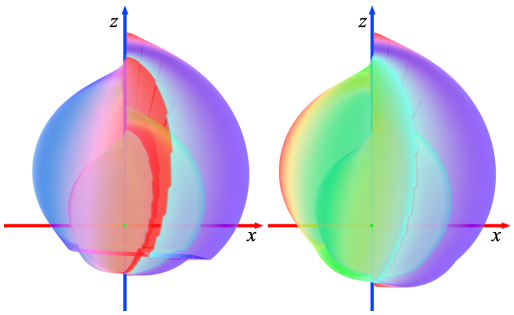

Figure 7: In the left figure, we see the sudden change of color of the semitransparent layer from red to blue color (see the electronic version). We also observe the discontinuity of the height of the semitransparent layer in the lower part of the visualization. The right figure shows the same object after the correct linking of the layers.

proves that the resulting function has two layers, each corresponding to one of the two branches $f(z)$ and $-f(z)$ of the square root function. When we encircle the point 0 along a image of a circle with the centre in point 0 in the clockwise direction, we see three repetitions of the color gradient, corresponding to z^3 in $f(z) = \sqrt{-z^3}$.

We also observe that the graph forms a cone around the point 0. This is due to the fact that 0 is also a branch point of the square root function as well, so the two layers of the graph meet at this point.

The color gradient is continuous in the entire visualization, indicating that the value of the argument of the function is also continuous. There are no discontinuities or leaps in the semitransparent layer, meaning that the value of the modulus of the function is also continuous. From the shape of the semitransparent layer we can also ascertain the direction of growth of the modulus of the function.

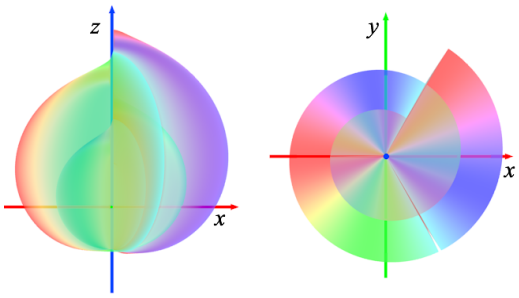

Figure 8: The graph of the function $f(z) = \sqrt{-z^3}$ from two different points of view: left the front view (the direction of view is the y-axis), right the top view (negative z-axis direction). The graph has two layers corresponding to the two branches of the square root function, and the color gradient repeats three times due to the 3rd power of z.

5 Deformations of ADE singularities and their visualizations

The technique of deformations is a fundamental method in e.g. algebraic geometry and related mathematical disciplines; in Computer Graphics, the deformations are used e.g. in morphing. However, the visualizations of deformations of complex functions are very scarce. So far, in the range of Computer Graphics, the approach similar to the proposed one is unknown to the authors. They are also not aware of any other work connecting singularities and complex function visualization in the presented way.

Loosely speaking, a deformation is a "slight change" of given object (e.g. of a curve or a function) in such a way, that the newly created object still carries enough information about the original one. The term "slight" can be on certain examples illustrated visually, but in general, this is not possible. The proper algebraic condition is expressed via the notion of *flatness* (see [Greuel et al. 2007]). For our purposes, the intuitive idea of a continuous transformation from one object to another suffices.

The complexity of given ADE singularity is given by its Milnor number, indicated by the subscript k. The presented continuous blend $A_k \to A_{k-1}$ allows us to decrease this number by one, which is the smallest possible step, up to regularity ($k = 0$); the animation comprehensibly captures the changes in the structure. Although the deformation $\sqrt{a(f-L)-f}$, where f is the original function, $a \in \langle 0,1 \rangle$ is the parameter and L a linear (=regular) function, is the most effective deformation in the sense that the singularity is removed in one step, this blend is not demonstrative enough, because the changes in the structure are not sufficiently detailed.

Here, we describe in detail the deformation between the A_2 and A_1 singularity in its normal form given by equation (3). For the sake of simplicity, we choose a 1-parameter deformation given by $f(z) = \sqrt{a(z^3-z^2)-z^3}$, where $a \in \langle 0,1 \rangle$ is the parameter. This system provides a decrease of the Milnor number by one. By changing the parameter, we get a sequence of images demonstrating the continuous changes of the topology between A_2 and A_1 singularity. In fig. 9, we see such a sequence for the sampled values of the parameter $a = 0, 0.4, 0.8, 1$.

In animations, we used an approximation of a sphere, where meridians are approximated by a polygonal line with 125 vertices and parallel lines approximated by a polygonal line with 250 vertices. To get a continuous final sequence, we changed the values of a from 0 to 1 by 0.01. That means, we get animation consisting of 100 different frames.

In fig. 9, the top left figure presents the function $f(z) = \sqrt{a(z^3-z^2)-z^3}$ for the parameter $a = 0$, i.e. $f(z) = \sqrt{-z^3}$ which is the cuspidal (see 3) curve with the A_2 singularity. The corresponding Riemann surface was described in detail in sec. 4.3. The next two figures illustrate the change between A_2 and A_1. We see that one singular point moves along the negative real axis from 0 to ∞. In the top right figure, we see the Riemann surface of the function $f(z) = \sqrt{-z^2}$, i.e. the curve containing the A_1 singularity at origin. Because the exponent is even, the surface consists of two separate parts, intersecting in the left side of the right-most figure. The graph has one singular point $z = 0$ and one singular point at the infinity.

In our work, we have also visualized the deformation between A_3 and A_2, see fig. 10.

6 Conclusion and future work

In this paper, we described and visualized the topology and structure of the ADE singularities in terms of the numerical and topological invariants such as Milnor number and its interpretation via

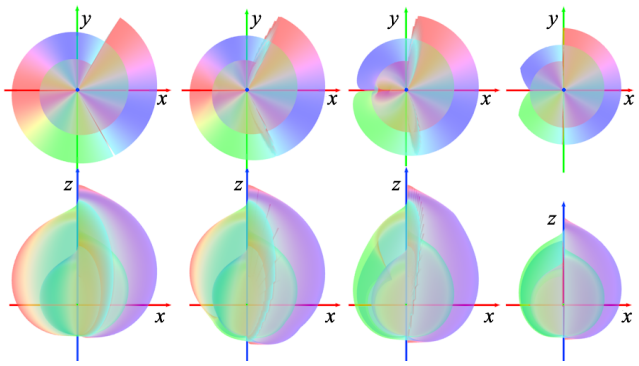

Figure 9: From left to right, the figure illustrates the changes of the graph of the deformation between the A_2 and A_1 singularities for the sampled values of the parameter $a = 0, 0.4, 0.8, 1$. In the top, the graph is displayed from the top, in the bottom, the graph from the front.

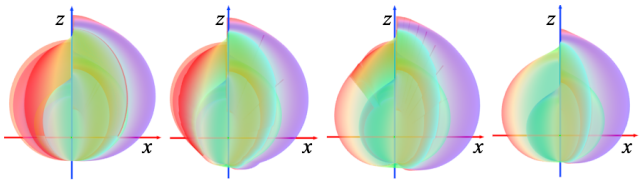

Figure 10: The figure depicts change between the A_3 and A_2 singularities for the sampled values of the parameter $a = 0, 0.4, 0.8, 1$.

knot associated with a singularity. In presence of more irreducible branches, a link has to be considered.

We used a 1-parameter system of deformations for their desingularization showing the local structure of the singularity. In an analogous way, the deformation of $A_k \to A_{k-1}$ can be constructed. We also handled the plane D_k singularities, because they are all reducible, with one of the components being regular and the other having an A_{k-3} singularity. The deformations of E_k are part of the future work.

We also used the notion of Riemann surfaces in order to propose a novel technique of visualization of multivalued complex functions. The novelty consists of displaying the whole domain of the function and extension of the existing domain coloring method with a specific height function.

Here, we focused on visualization of singularities of plane algebraic curves, thus a natural extension leads to visualization of singularities of curves lying on an algebraic surface. It is also planned to consider the deformations for surfaces with isolated singularities given by equations analogous to equations (3).

Technically, the visualization will be adapted using subdivision of the mesh and alternative ways of meshing of the sphere, and using antialiasing techniques in order to reduce complexity of computations in models and animations.

7 Acknowledgment

The authors have been supported by the projects *VEGA 1/0330/13*, *UK/465/2013* and *ASFEU Comeniana – methods and means of presentation and digitization of 3D cultural heritage objects,* OPVaV-2011/4.2/07-SORO, ITMS: 26240220077.

References

BLENDER, 2013. Blender. `http://www.blender.org/`.

BRIESKORN, E., AND KNÖRRER, H. 1986. *Plane Algebraic Curves*. Birk-Häuser Verlag Basel, New York.

FARRIS, F. A., 2012. Visualizing complex-valued functions in the plane. `http://www.maa.org/pubs/amm_complements/complex.html`.

FORSTER, O. 1981. *Lectures on Riemann Surfaces (Graduate Texts in Mathematics)*. Springer.

GREUEL, G. M., LOSSEN, C., AND SHUSTIN, E. 2007. *Introduction to Singularities and Deformations*. Springer-Verlag New York Inc., New York.

HASSET, B. 2000. Local stable reduction of plane curve singularities. *Journal für die reine und angewandte Mathematik (Crelles Journal) 520*, 169–194.

JONES, G. A., AND SINGERMAN, D. 1987. *Complex functions: an algebraic and geometric viewpoint*. Press Syndicate of the University of Cambridge, Great Britain.

LANG, S. 1999. *Complex Analysis, Fourth Edition*. Springer, New York, USA.

LUNDMARK, H., 2004. Visualizing complex analytic functions using domain coloring. `http://www.mai.liu.se/~halun/complex/domain_coloring-unicode.html`.

MAXIMA, 2012. Maxima. `http://maxima.sourceforge.net/`.

NEEDHAM, T. 2000. *Visual Complex Analysis*. Oxford University Press Inc., New York, USA.

NIESER, M., POELKE, K., AND POLTHIER, K. 2010. Automatic generation of Riemann surface meshes. In *Advances in Geometric Modeling and Processing*, B. Mourrain, S. Schaefer, and G. Xu, Eds., vol. 6130 of *Lecture Notes in Computer Science*. Springer Berlin / Heidelberg, 161–178.

POELKE, K., AND POLTHIER, K. 2009. Lifted domain coloring. *Computer Graphics Forum 28*, 3, 735–742.

PYTHON, 2012. Python. `http://www.python.org/`.

TROTT, M., 2002. Visualization of Riemann surfaces IId. `http://www.mathematica-journal.com/issue/v8i4/columns/trott/contents/RiemannIId.pdf`.

VALÍKOVÁ, M., AND CHALMOVIANSKÝ, P. 2010. Visualization of complex functions on the Riemann sphere (in slovak). *In Proceedings of Symposium on Computer Geometry SCG 2010 19*, 87–92.

VALÍKOVÁ, M., AND CHALMOVIANSKÝ, P. 2012. Visualization of the multivalued complex functions using the Riemann surfaces in slovak. *In Proceedings of Symposium on Computer Geometry SCG 2012 21*, 120–125.

WALL, C. T. C. 2004. *Singular points of algebraic curves*. Cambridge University Press, New York.

WOLFRAM RESEARCH, I., 2013. Mathematica. `http://www.wolfram.com/mathematica/`.

YIN, X., JIN, M., AND GU, X. 2007. Computing shortest cycles using universal covering space. In *CAD/Graphics*, IEEE, 25.